SCIENCE CHINA
Technological Sciences

November 2011 Vol.54 No.11: 2974–2980
doi: 10.1007/s11431-011-4453-6

Research on hovering control scheme to non-circular orbit

WANG GongBo, ZHENG Wei*, MENG YunHe & TANG GuoJian

College of Aerospace and Material Engineering, National University of Defense Technology, Changsha 410073, China

Received December 6, 2010; accepted April 11, 2011

An open-loop control system for hovering at any selected position on spacecraft orbit is first presented given that the satellite's engine provides continuous finite thrust. Actually, the hovering states are unstable considering perturbations and thrust errors, so a feedback sliding mode variable structure control, which is adaptive and chattering-free, is designed. Under this feedback control scheme, the high-frequency chattering phenomenon is avoided, while the system stays highly robust at the same time. Simulation results show that the feedback control thrusts are continuous and the steady-states error can be confined to 10^{-4} m at the presence of uncertain perturbations. Finally, the feasibility of realizing hovering orbits is analyzed taking the "Moliya" and geosynchronous Earth orbit (GEO) satellites as examples.

continuous finite thrust, hovering orbit, chattering-free, variable structure control

Citation: Wang G B, Zheng W, Meng Y H, et al. Research on hovering control scheme to non-circular orbit. Sci China Tech Sci, 2011, 54: 2974–2980, doi: 10.1007/s11431-011-4453-6

1 Introduction

"Hovering orbit" is the orbit of the active satellite which holds still relative to some space target. Due to the precious character of relative stillness, hovering orbit has a bright future in space missions [1, 2], such as interfering communication by hovering to communication satellite towards the side of Earth, expanding the space resources of GEO, and hovering formation flying on hyperbolic orbits of deep space missions, which can expand the baseline of measurement.

There are two kinds of work of hovering orbits, hovering to asteroids and hovering to near Earth satellites.

Sawai et al. [3] studied the control of a spacecraft hovering over a uniformly rotating asteroid using altimetry. Broschart [4] investigated the stability of realistic hovering control laws in the small-body-fixed and inertial reference frames. Lu [5] presented that it might be used to deflect small Earth-approaching asteroids' orbits to avoid possible impaction using the gravity between asteroid and spacecraft which is hovered to the asteroid at right position.

Most of resent researches on hovering orbits to near Earth satellites focused on circle orbits.

Lin [6] studied the method to hover to target spacecrafts of circle orbits in the radial direction. Yan [7] expanded the hovering position, and gave a geometry method to realize hovering to circle orbits at any position. Li [8] analyzed the initial and control method of hovering formation using Hill equations.

Actually, ideal circle orbits don't exist because of perturbations, and the solutions based on circle orbits mentioned above are not quite suitable to realistic space missions. Therefore, it is necessary to study the hovering method to target spacecrafts on elliptic and hyperbolic orbits. We presented an open loop orbit control strategy to maintain hovering at any selected position to elliptical orbit in ref. [9] based on dynamics theory, and supposed that the satellite's engine provides continuous finite thrust. However, the open loop control method is not stable due to perturba-

*Corresponding author (email: nudt1304@163.com)

tions and thrust errors, and feedback control laws are badly needed to keep the hovering states stable.

Based on the results of ref. [9], a feedback sliding mode variable structure control scheme which is adaptive and chattering-free is mainly designed in this paper. The relationship among precise, control parameters and fuel consumption is also discussed, and simulation results show that the feedback control law is effective.

2 Open-loop control method

2.1 Definition of coordinates

Typically, a relative orbit is sensed or measured in terms of the local-vertical-local-horizon (LVLH) coordinates, which are denoted as S-*xyz* in Figure 1, in which S denotes reference satellite and C represents company satellite. Subscript S denotes reference satellite quantities and subscript C indicates company satellite quantities. The rotating LVLH coordinate frame has it's *x* axis aligned with the reference's radial position vector and the *z* axis aligned with angular momentum vector. $\boldsymbol{r}$ is the position vector, and $\boldsymbol{l}$ is the relative position vector. The relationship between $\boldsymbol{r}$ and $\boldsymbol{l}$ can be written as

$$\boldsymbol{r}_{\mathrm{c}} = \boldsymbol{r}_{\mathrm{s}} + \boldsymbol{l}. \tag{1}$$

Let $\boldsymbol{r}_{\mathrm{s}}$ be $\boldsymbol{r}_{\mathrm{s}} = (r_{\mathrm{s}} \quad 0 \quad 0)^{\mathrm{T}}$ and $\boldsymbol{l}$ be $\boldsymbol{l} = (x \quad y \quad z)^{\mathrm{T}}$ in terms of LVLH coordinates. $\boldsymbol{r}_{\mathrm{c}}$ can be written as $\boldsymbol{r}_{\mathrm{c}} = (r_{\mathrm{s}} + x \quad y \quad z)^{\mathrm{T}}$.

2.2 Open-loop control equations

The open-loop hovering control equation of elliptic orbits is given in ref. [9] as

$$\boldsymbol{a}_{\mathrm{control}} = \frac{\mu}{r_{\mathrm{s}}^3}\begin{pmatrix} -2x \\ y \\ z \end{pmatrix} + \varepsilon\begin{pmatrix} -y \\ x \\ 0 \end{pmatrix} - \omega^2\begin{pmatrix} x \\ y \\ 0 \end{pmatrix}, \tag{2}$$

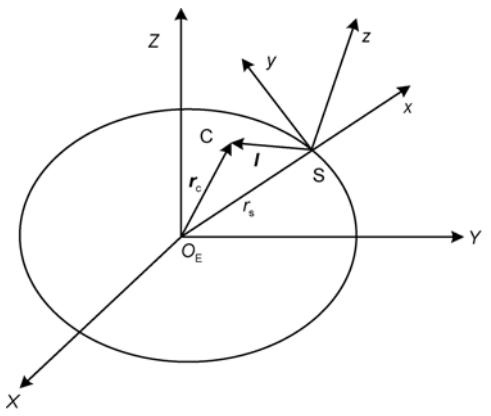

Figure 1 Earth inertial Cartesian coordinates and LVLH coordinates.

where $\boldsymbol{a}_{\mathrm{control}}$ is the control acceleration, and μ is the Earth gravity constant. ω and ε denote angular velocity and acceleration, respectively, and can be written as

$$\omega = \dot{f} = h/r_{\mathrm{s}}^2, \tag{3}$$

$$\varepsilon = -2\frac{\mu}{r_{\mathrm{s}}^3}\cdot e\sin f, \tag{4}$$

where $h = \sqrt{a\mu(1-e^2)}$ is the angular momentum. *a*, *e* and *f* represent the semi-major axis, eccentricity and true anomaly, respectively.

2.3 Fuel consumption

Let *T* be the orbital period, $T=2\pi/n_{\mathrm{s}}$, in which $n_{\mathrm{s}} = \sqrt{\mu/a^3}$ denotes the mean angular velocity of the reference satellite. The velocity increment during an orbital period can be expressed as

$$\Delta v_T = \int_0^T \left|\boldsymbol{a}_{\mathrm{control}}\right| \mathrm{d}t. \tag{5}$$

The velocity increments of three coordinate directions are given in ref. [9] as

$$\Delta v_{Tx} = -2\pi x n_{\mathrm{s}}\left(3+\frac{1}{2}e^2\right)\left(1-e^2\right)^{-\frac{3}{2}}, \tag{6}$$

$$\Delta v_{Ty} = -4n_{\mathrm{s}}e\left(1-e^2\right)^{-\frac{3}{2}}\sqrt{4x^2+y^2}, \tag{7}$$

$$\Delta v_{Tz} = 2\pi z n_{\mathrm{s}}\left(1-e^2\right)^{-\frac{3}{2}}. \tag{8}$$

Supposing that the reference orbit is circle, we can get $\varepsilon=0$ and $\omega^2 = \mu/r_{\mathrm{s}}^3$, then the control acceleration can be simplified as

$$\boldsymbol{a}_{\mathrm{control}} = \omega^2\left[-3x \quad 0 \quad z\right]^{\mathrm{T}}, \tag{9}$$

and the velocity increments of an orbital period are

$$\Delta v_{Tx} = 6\pi n_{\mathrm{s}} x,\ \Delta v_{Tz} = 2\pi n_{\mathrm{s}} z. \tag{10}$$

If the reference orbit is hyperbolic, for leading-following hovering formation, which has

$$\boldsymbol{l} = (0 \quad y \quad 0)^{\mathrm{T}}, \tag{11}$$

the velocity increments are

$$\Delta v_{Tx} = 2y\sqrt{\frac{\mu}{p^3}}\left(e+1\right)^2, \tag{12}$$

$$\Delta v_{Ty} = y\sqrt{\frac{\mu}{p^3}}\left(e^2 f_{\infty} + \sqrt{e^2-1}\right), \tag{13}$$

where f_∞ is the true anomaly at infinite distance, and p is the semilatus rectum. According to the definition of hyperbola, it is easy to get

$$\cos f > -\frac{1}{e}, \tag{14}$$

and

$$f_\infty = \cos^{-1}\left(-\frac{1}{e}\right). \tag{15}$$

3 Feedback control scheme design

The control eq. (2) is derived under the assumption of two-body, actually the hovering formation with this control method will gradually be destroyed by perturbations. Therefore, feedback control laws must be applied to keep the formation stable. However, the perturbations are very complex, and it is hard to build accurate models for them. So, the quantity of anti-jamming becomes the most important performance of the feedback scheme.

Sliding mode variable structure control is widely concerned due to its highly robust character, however, the high-frequency chattering phenomenon caused by the inertial of realistic switches restricts the application of variable structure control a lot. To solve this problem, an adaptive chattering-free variable structure control scheme is developed in the following sections, which can almost eliminate chattering phenomenon and stay highly robust.

3.1 State equation

Let the relative position vector of hovering satellite be

$$\boldsymbol{X}_1 = (x \quad y \quad z)^{\mathrm{T}}, \tag{16}$$

and the relative velocity vector be

$$\boldsymbol{X}_2 = \dot{\boldsymbol{X}}_1 = (\dot{x} \quad \dot{y} \quad \dot{z})^{\mathrm{T}}. \tag{17}$$

The relative acceleration vector can be expressed as

$$\dot{\boldsymbol{X}}_2 = f(t,\boldsymbol{X}) + \boldsymbol{B}(t,\boldsymbol{X})\boldsymbol{U} + \Delta f(t,\boldsymbol{X},\boldsymbol{U}), \tag{18}$$

where $\Delta f(t, \boldsymbol{X}, \boldsymbol{U})$ denotes the part of relative acceleration which can not be modeled, and $\boldsymbol{U}$ indicates the control vector which can be separated into two parts

$$\boldsymbol{U} = \boldsymbol{U}_{\mathrm{d}} + \boldsymbol{U}_{\mathrm{c}}, \tag{19}$$

where $\boldsymbol{U}_{\mathrm{c}}$ represents the feedback control vector, and $\boldsymbol{U}_d$ denotes the standard open-loop control vector, which is

$$\boldsymbol{U}_{\mathrm{d}} = \boldsymbol{a}_{\mathrm{control}}. \tag{20}$$

Using T-H eq. [10], we can get

$$f(t,\boldsymbol{X}) = \boldsymbol{A}_1\boldsymbol{X}_1 + \boldsymbol{A}_2\boldsymbol{X}_2, \tag{21}$$

$$\boldsymbol{B}(t,\boldsymbol{X}) = \begin{bmatrix} 1 & 0 & 0 \\ 0 & 1 & 0 \\ 0 & 0 & 1 \end{bmatrix}, \tag{22}$$

where

$$\boldsymbol{A}_1 = \begin{bmatrix} \omega^2 + 2c_{\mathrm{s}} & \varepsilon & 0 \\ -\varepsilon & \omega^2 - c_{\mathrm{s}} & 0 \\ 0 & 0 & -c_{\mathrm{s}} \end{bmatrix}, \tag{23}$$

$$\boldsymbol{A}_2 = \begin{bmatrix} 0 & 2\omega & 0 \\ -2\omega & 0 & 0 \\ 0 & 0 & 0 \end{bmatrix}, \tag{24}$$

c_{s} can be expressed as $c_{\mathrm{s}} = n_{\mathrm{s}}^2\left(\dfrac{1+e\cos f}{1-e^2}\right)^3$.

So far, the states equation can be written in term of chaos [11] as

$$\begin{cases} \boldsymbol{X}_2 = \dot{\boldsymbol{X}}_1, \\ \dot{\boldsymbol{X}}_2 = f(t,\boldsymbol{X}) + \boldsymbol{B}(t,\boldsymbol{X})\boldsymbol{U} + \Delta f(t,\boldsymbol{X},\boldsymbol{U}), \\ \boldsymbol{Y} = \boldsymbol{X}_1. \end{cases} \tag{25}$$

3.2 Expanded state equation

Supposing that

$$\boldsymbol{X}_3 = \dot{\boldsymbol{X}}_2, \tag{26}$$

we can immediately have

$$\dot{\boldsymbol{X}}_3 = F(t,\boldsymbol{X}) + \dot{\boldsymbol{U}} + \Delta F(t,\boldsymbol{X},\boldsymbol{U}), \tag{27}$$

where

$$F(t,\boldsymbol{X}) = \frac{\mathrm{d}f(t,\boldsymbol{X})}{\mathrm{d}t}, \tag{28}$$

$$\Delta F(t,\boldsymbol{X},\boldsymbol{U}) = \frac{\mathrm{d}\Delta f(t,\boldsymbol{X},\boldsymbol{U})}{\mathrm{d}t}. \tag{29}$$

Substituting eqs. (26)–(29) into eq. (25) leads to the expanded state equation in terms of chaos

$$\begin{cases} \boldsymbol{X}_{i+1} = \dot{\boldsymbol{X}}_i, \quad 1 \leqslant i \leqslant 2, \\ \dot{\boldsymbol{X}}_3 = F(t,\boldsymbol{X}) + \dot{\boldsymbol{U}}_{\mathrm{d}} + \boldsymbol{v}_{\mathrm{c}} + \Delta F(t,\boldsymbol{X},\boldsymbol{U}), \\ \boldsymbol{Y} = \boldsymbol{X}_1. \end{cases} \tag{30}$$

3.3 Sliding mode variable structure control scheme design

The control scheme is designed for the states equation of

eq. (30).

3.3.1 Sliding surface design

The sliding variable is chosen as

$$\boldsymbol{s} = \ddot{\boldsymbol{e}} + \boldsymbol{c}_1\dot{\boldsymbol{e}} + \boldsymbol{c}_2\boldsymbol{e}, \tag{31}$$

where

$$\boldsymbol{e} = \boldsymbol{X}_{\mathrm{d}} - \boldsymbol{X}_1, \tag{32}$$

where $\boldsymbol{X}_{\mathrm{d}}$ denotes the expected hovering position. Eq. (31) depicts a typical second-order system. $\boldsymbol{c}_1$ and $\boldsymbol{c}_2$ are both diagonally matrix, which can be solved according to expected dynamic characteristics.

3.3.2 Reaching law design

Saturation function is used to weaken chattering, which is

$$sat\left(s_j,\varepsilon\right) = \begin{cases} \mathrm{sgn}\left(s_j\right), & \left|s_j\right| > \varepsilon, \\ s_j/\varepsilon, & \left|s_j\right| \leqslant \varepsilon, \end{cases} \quad j = 1,2,3. \tag{33}$$

The reaching law of ref. [12] is adopted, which is

$$\dot{\boldsymbol{s}} = -k \cdot sat\left(\boldsymbol{s},\varepsilon\right) - r \cdot \boldsymbol{s}, \tag{34}$$

where $k > 0$ and $r > 0$ must be satisfied.

In the following, the equal control law $\boldsymbol{v}_{\mathrm{eq}}$ on sliding surface is first solved. During the sliding mode, the variable must meet

$$\dot{\boldsymbol{s}} = 0. \tag{35}$$

Substituting eqs. (30)–(32) into eq. (35), we can get

$$\ddot{\boldsymbol{X}}_{\mathrm{d}} - \left(\boldsymbol{F}\left(t,\boldsymbol{X}\right) + \dot{\boldsymbol{U}}_{\mathrm{d}} + \boldsymbol{v}_{\mathrm{eq}}\right) + \boldsymbol{c}_1\ddot{\boldsymbol{e}} + \boldsymbol{c}_2\dot{\boldsymbol{e}} = 0. \tag{36}$$

Therefore, the equal control law $\boldsymbol{v}_{\mathrm{eq}}$ can be written as

$$\boldsymbol{v}_{\mathrm{eq}} = \ddot{\boldsymbol{X}}_{\mathrm{d}} - \boldsymbol{F}\left(t,\boldsymbol{X}\right) - \dot{\boldsymbol{U}}_{\mathrm{d}} + \boldsymbol{c}_1\ddot{\boldsymbol{e}} + \boldsymbol{c}_2\dot{\boldsymbol{e}}. \tag{37}$$

Then, the variable structure control law $\Delta\boldsymbol{v}$ will be derived which can drive the system to sliding mode. The sliding variable should meet eq. (34) while the system is not in the sliding mode. Substituting eqs. (30)–(32) into eq. (34), we can get

$$\begin{aligned} &\ddot{\boldsymbol{X}}_{\mathrm{d}} - \left(\boldsymbol{F}\left(t,\boldsymbol{X}\right) + \dot{\boldsymbol{U}}_{\mathrm{d}} + \boldsymbol{v}_{\mathrm{eq}} + \Delta\boldsymbol{v} + \Delta\boldsymbol{F}\left(t,\boldsymbol{X}\right) + \boldsymbol{c}_1\ddot{\boldsymbol{e}} + \boldsymbol{c}_2\dot{e}\right) \\ &= -k \cdot sat\left(\boldsymbol{s},\varepsilon\right) - r \cdot \boldsymbol{s}. \end{aligned} \tag{38}$$

Substituting eq. (37) into eq. (38) yields the variable structure control law $\Delta\boldsymbol{v}$ as

$$\Delta\boldsymbol{v} = k \cdot sat\left(\boldsymbol{s},\varepsilon\right) + r \cdot \boldsymbol{s}. \tag{39}$$

According to eqs. (37) and (39), the variable structure control scheme for expanded system can be written as

$$\boldsymbol{v}_{\mathrm{c}} = \boldsymbol{v}_{\mathrm{eq}} + \Delta\boldsymbol{v}, \tag{40}$$

which can also be expressed as

$$\begin{aligned} \boldsymbol{v}_{\mathrm{c}} = {} & \ddot{\boldsymbol{X}}_{\mathrm{d}} - \boldsymbol{F}\left(t,\boldsymbol{X}\right) - \dot{\boldsymbol{U}}_{\mathrm{d}} + \boldsymbol{c}_1\ddot{\boldsymbol{e}} + \boldsymbol{c}_2\dot{\boldsymbol{e}} \\ & + k \cdot sat\left(\boldsymbol{s},\varepsilon\right) + r \cdot \boldsymbol{s}. \end{aligned} \tag{41}$$

The variable structure control law for the original system denoted by eq. (25) is the integral of eq. (41), which is

$$\begin{aligned} \boldsymbol{U}_{\mathrm{c}} = {} & \ddot{\boldsymbol{X}}_{\mathrm{d}} - f\left(t,\boldsymbol{X}\right) - \boldsymbol{U}_{\mathrm{d}} + \boldsymbol{c}_1\dot{\boldsymbol{e}} + \boldsymbol{c}_2\boldsymbol{e} \\ & + k\int_0^t sat\left(\boldsymbol{s},\varepsilon\right)\mathrm{d}t + r\int_0^t \boldsymbol{s}\mathrm{d}t. \end{aligned} \tag{42}$$

By substituting eq. (21) into eq. (42), it can be simplified into

$$\begin{aligned} \boldsymbol{U}_c = {} & \left(\boldsymbol{A}_1 + \boldsymbol{c}_2\right)\boldsymbol{e} + \left(\boldsymbol{A}_2 + \boldsymbol{c}_1\right)\dot{\boldsymbol{e}} \\ & + k\int_0^t sat\left(\boldsymbol{s},\varepsilon\right)\mathrm{d}t + r\int_0^t \boldsymbol{s}\mathrm{d}t. \end{aligned} \tag{43}$$

Comparing eq. (41) and eq. (43), we can find the followings.

1) Saturation function is brought into eq. (41), which can weaken the chattering in some degree, but for discrete system it can not make sure that the control thrust is continuous.

2) Based on eq. (41), integral is further used in eq. (43) which is more effective to eliminate the high-frequency chattering phenomenon.

The system of eq. (25) is stable under the control of eq. (43), and arbitrarily desired tracking accuracy can be achieved within a finite time if the parameter of the control scheme is appropriately set. See details in ref. [12].

The sliding surface and parameters of reaching law are key factors in variable structure control, which decide the precision and quality, so the value of k in eq. (43) should be well considered. Increasing the value of k, the reaching movement will be more fast, which enhances the quality of robustness but reduces the steady-state precision. It will be helpful to decrease the value of k to raise the steady-state precision, but the time of convergence will be delayed at the same time, even making it impossible to reach sliding mode in some worst situations. To solve this contradiction, an attenuation factor λ ($0 < \lambda < 1$) is brought into k, which was proposed in ref. [13], and k is expressed as

$$\begin{cases} k\left(i+1\right) = \lambda k\left(i\right), & \left|\min s_j\right| > \varepsilon, \\ k\left(i+1\right) = k\left(i\right), & \left|\max s_j\right| < \varepsilon, \end{cases} \quad j = 1,2,3. \tag{44}$$

4 Simulations

Three different types of reference orbits are chosen to realize hovering formation, which are highly elliptic: “Molniya” communication satellite (S1), circle GEO satellite (S2) and

hyperbolic Lunar detector (S3). The initial orbit elements are shown in Table 1, and the data of S3 are measured in Lunar-centered inertial frame.

4.1 Open-loop controller

Suppose that the target hovering position vector of S1 is $\boldsymbol{l}_1 = (-1000 \quad 0 \quad 0)^{\mathrm{T}}$. The control acceleration which is the function of true anomaly f can be obtained from eq. (2) as

$$\boldsymbol{a}_{\text{control}} = 2.32\times10^{-4}\cdot\begin{pmatrix}3+0.74\cos f\\ 1.48\sin f\\ 0\end{pmatrix}\cdot(1+0.74\cos f)^3. \quad (45)$$

The relationship between acceleration and true anomaly is shown in Figure 2, from which we can see that the minimum of total acceleration is approximately 9.11×10^{-6} m s^{-2}, coming up at the apogee.

According to eqs. (6)–(8), the velocity increments of three coordinate directions in a orbital period are Δv_{Tx} = 9.915 m s^{-1}, Δv_{Ty}=2.857 m s^{-1} and Δv_{Tz}=0, with total increment Δv_T=10.317 m s^{-1}.

Assuming that the target hovering position vector of S2 is $\boldsymbol{l}_2 = (0 \quad 0 \quad 1000)^{\mathrm{T}}$, the control acceleration is simplified as constant value along the z direction, with the value of a_z=5.289×10^{-6} m s^{-1}. The velocity increment per day is 0.457 m s^{-1}.

Let the azimuth be α ($\alpha \in [0, 2\pi]$), which is defined as the angle measured from the y axis to the projection of relative position vector on the local horizon plane. β ($\beta \in [-1/2\,\pi, 1/2\,\pi]$) denotes the altitude angle, which is defined as the angle between the relative position vector and the local horizon plane. The relative position vector can be written as $\boldsymbol{l} = l(\sin\beta \quad \cos\beta\sin\alpha \quad \cos\beta\cos\alpha)^{\mathrm{T}}$. The velocity increments per day at different positions are shown in Figure 3.

Suppose that the target hovering position vector of S3 is $\boldsymbol{l}_3 = (0 \quad 1000 \quad 0)^{\mathrm{T}}$, and that the relationship between acceleration and true anomaly is shown in Figure 4. The velocity increments in a orbital period are Δv_{Ty}=10.259 m s^{-1}, Δv_{Ty}=5.166 m s^{-1}, with total increment Δv_T=11.486 m s^{-1}. From eq. (12), we know that the velocity increment is the function of perilune altitude and eccentricity, which is shown clearly in Figure 5.

Tabel 1 Initial orbit elements of reference satellites

Elements	S1	S2	S3
a (km)	26553.375	42241.098	−1550.400
e	0.741	0	1.500
i (°)	63.400	0	23.500
w (°)	270.000	0	270.000
Ω (°)	−30.520	60.000	0
f (°)	0	0	−131.810

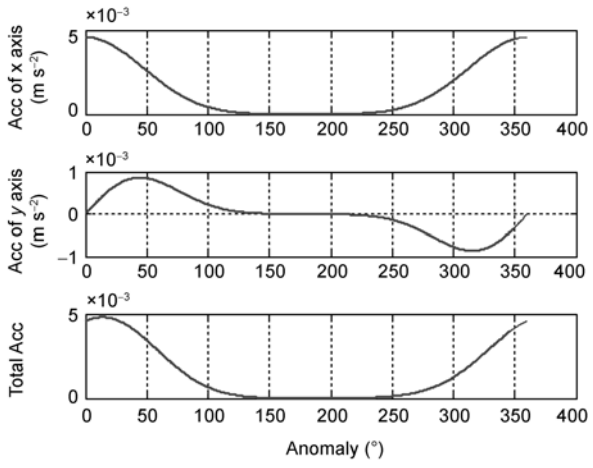

Figure 2 Relationship between acceleration and true anomaly (S1).

4.2 Feedback controller

The sliding mode variable structure control depicted as eq. (43) will be used to maintain the hovering formation stable. The control parameters are chosen as ε=10^{-4}, λ=0.9995, k=r=10^{-6}, c_1=diag (8 8 8)×10^{-2}, and c_2=diag (1 1 1) ×10^{-3}. The initial value of the integral term is set as 10^{-4}, and the initial position err is 10 m, with simulation step 0.1 s. The unknown terms are given as

$$\Delta f(t, \boldsymbol{X}, \boldsymbol{U}) = 10^{-5}\cdot\sin t. \quad (46)$$

The relative range errors under feedback control are given in Figures 6 and 7, with the steady error less than 10^{-4} m. The real relative states are yielded as follows. First, the orbit elements of both company and reference satellites in inertial frame are calculated, then we can get the relative states in terms of inertial frame. Through frame transition between Earth-centered inertial coordinate and LVLH, we can finally have the relative states in LVLH coordinates. Perturbations during the computation include non-spherical of 21×21 terms, solar radiation, atmosphere drag and the third body gravity.

Figure 8 shows the feedback control thrust in one period, and the thrusts of y and z axes are local, from which we can see that the control thrust is continuous and the chattering phenomenon is eliminated. The total fuel consumption of the feedback control in one orbital period is approximately 0.345 m s^{-1}.

Figure 9 depicts the changing curve of the sliding variable s, and the graph of y and z axes are local, from which we can find that the sliding variable is also continuous and is confined to less than 10^{-7}.

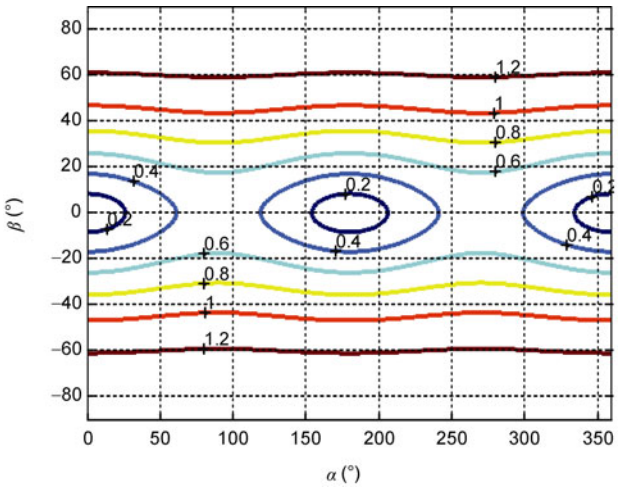

Figure 3 Velocity increment contour lines during a orbital period (S2).

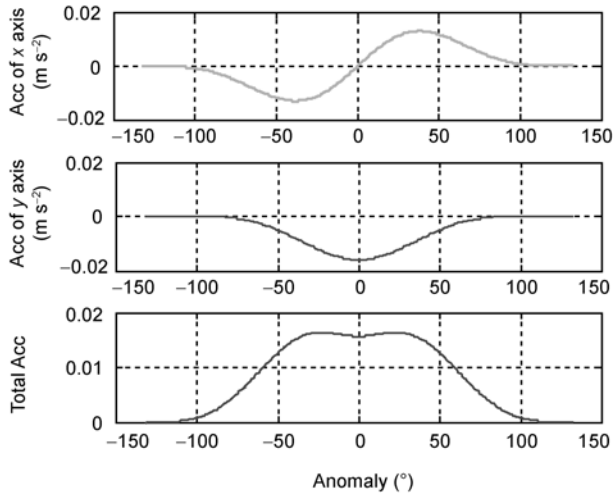

Figure 4 Relationship between acceleration and true anomaly (S3).

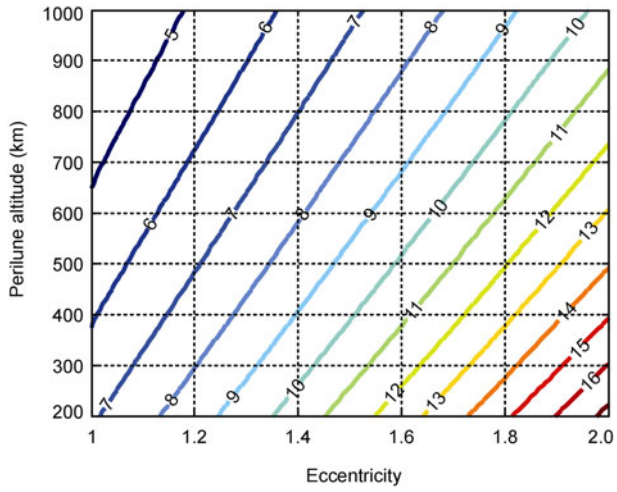

Figure 5 Velocity increment contour lines vs. eccentricity and perilune altitude (S3).

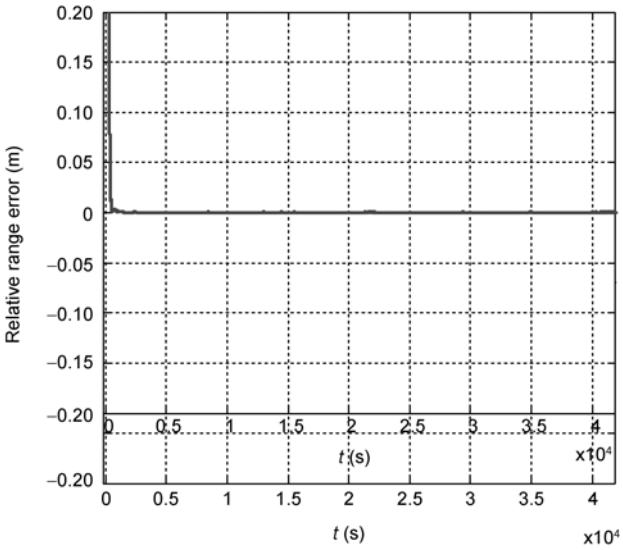

Figure 6 Relative range errors.

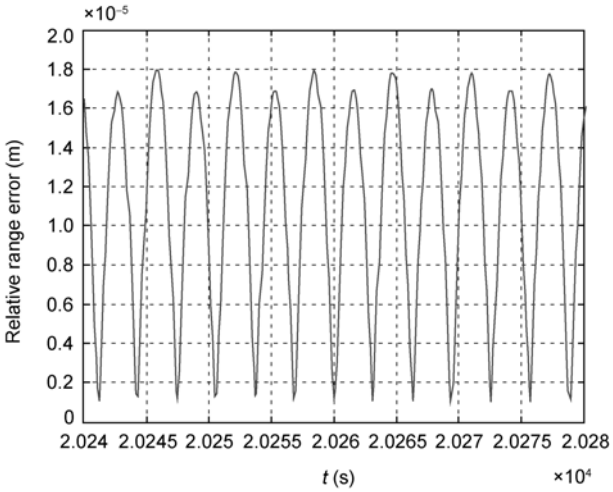

Figure 7 Relative range errors (local).

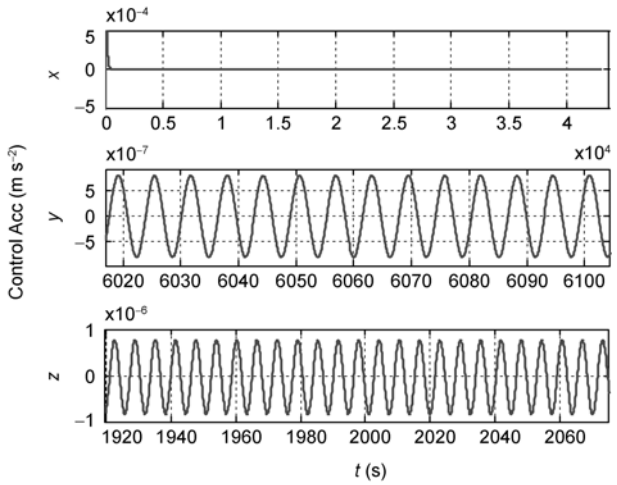

Figure 8 Feedback control thrusts.

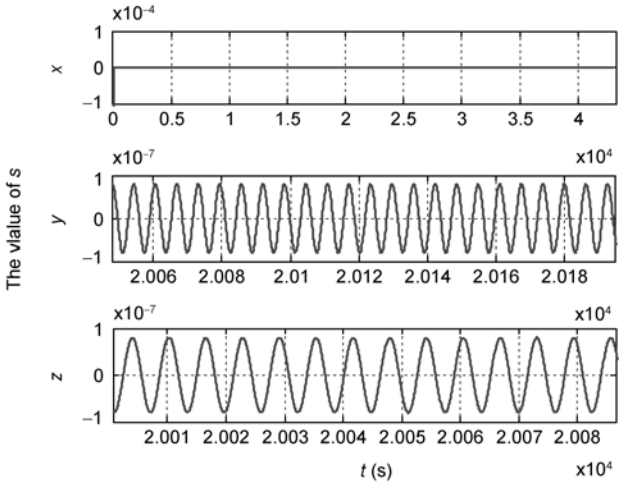

Figure 9 The value of function *s*.

4.3 Analysis of total fuel consumption

In this section, the feasibility of realizing hovering orbits is analyzed taking the S1 and S2 satellites as example.

Let the mass of reference satellite be m_s, designed life-span be T_d, velocity increment per day of unit mass be Δv, total fuel consumption be Δm, and the exhaust velocity be v_e. Then we can get

$$\Delta m v_e \approx \Delta v \cdot m_s \cdot T_d. \tag{47}$$

Given the mass of satellite S1 m_{s1}=1000 kg, the velocity increment of open-loop control in one orbital period is 10.317 m s^{-1}, while the feedback control needs 0.345 m s^{-1}. The total velocity increment of unit mass per day is

$$\Delta v_{s1} = (10.317 + 0.345) \times 2 = 21.324 \text{ m s}^{-1}. \tag{48}$$

Given the mission that disturbs the communication of S1 for 100 days, the life-span of the mission is T_{d1}=100 d. Taking GOCE (Gravity field and steady-state Ocean Circulation Explorer) [14] for example, which is equipped with xenon ions propulsions with exhaust velocity exceeding 40000 m s^{-1}. Substituting T_{d1}=100 d and v_e=40000 m s^{-1} into eq. (47), we can yield the total fuel consumption to be $\Delta m_{s1} \approx 53.310$ kg.

Given the mass of satellite S2 m_{s2}=1000 kg, the velocity increment of open-loop control in one orbital period is 0.457 m s^{-1}. The unknown perturbations of high orbits are smaller than low orbits, which can be chosen as

$$\Delta f(t, \boldsymbol{X}, \boldsymbol{U}) = 10^{-6} \cdot \sin t. \tag{49}$$

The initial position error is set to be 10 m. The velocity increment of feedback control in the first orbital period is 0.347 m s^{-1}, which will be reduced to 0.014 m s^{-1} per day after the first period. So, the total velocity increment of unit mass per day can be easily calculated as $\Delta v_{s2} \approx 0.471$ m s^{-1}. Supposing that T_{d2}=5 a, the total fuel consumption can be obtain as $\Delta m_{s2} \approx 21.5$ kg, which is less than 3% of the mass of the entire satellite. With GEO satellites launched more and more, this kind of space resource becomes much more precious, which makes the research of hovering orbits much more meaningful.

5 Conclusions

1) An open-loop hovering control strategy is proposed which might be applied to any kind of orbits.

2) A feedback sliding mode variable structure control scheme is designed, under which the chattering phenomenon is avoided while the system stays highly robust at the same time.

3) To hover right below the "Molniya" communication satellite at a distance of 1 km, the velocity increment needed by feedback control in one orbital period is 0.345 m s^{-1}, with steady error less than 10^{-4} m. The fuel consumption is 53.3 kg given the mass of hovering satellite 1000 kg and the life-span 100 d.

4) To hover to GEO satellite in the normal direction at the distance of 1 km for 5 a, the fuel required is 21.5 kg if the hovering satellite's mass is 1000 kg.

This work was supported by the National Natural Science Foundation of China (Grant No. 10702078) and the National Basic Research Program of China ("973" Program) (Grant No. JC08-01-05).

1 Yuan J P, Zhu Z X. Space operations and non-Keplerian orbit motion. J Astron, 2009, 30(1): 42–46
2 Wang P, Yuan J P, Fan J F. Discussion on non-Keplerian orbit. J Astron, 2009, 30(1): 37–41
3 Sawai S, Scheeres D J, Broschart S B. Control of hovering spacecraft using altimetry. J Guid Contr Dynam, 2002, 25(4): 786–795
4 Broschart S B, Scheeres D J. Control of hovering spacecraft near small bodies: Application to asteroid 25143 Itokawa. J Guid Contr Dynam, 2005, 28(2): 343–354
5 Lu E, Love S. Gravitational tractor for towing asteroids. Nature, 2005, 438(11): 177–178
6 Lin L X, Li K. Orbit dynamics and control of satellites hovering over space target. Chin Space Sci Tech, 2008, 28(2): 9–12
7 Yan Y. Study of hovering method at any selected position to space target. Chin Space Sci Tech, 2009, 29(1): 1–5
8 Li Y K, Jing Z L, Hu S Q. Relative dynamics hovering control with continuous finite thrust for circular orbital target. In: Proc. of Space Non-Keplerian Orbit Dynamics and Control Conference, Harbin, 2008
9 Wang G B, Meng Y H, Zheng W, et al. Research of hovering method to elliptical orbit based on dynamics. J Astron, 2010, 31(6): 1527–1532
10 Inalhan G, Tillerson M, How J P. Relative dynamics and control of spacecraft formations in eccentric orbits. J Guid Contr Dynam, 2002, 25(1): 48–59
11 Yu D C, Meng Q H. A novel sliding mode nonlinear proportional-integral control scheme for controlling chaos. Chin Phys, 2005, 14(5): 914–921
12 Gao W B. Theory and Design of Variable Structure Control. Beijing: Science Press, 1996
13 Zhang Y L, Zeng G Q, Wang Z K, et al. Theory and Application of Distributed Satellites System. Beijing: Science Press, 2008
14 Wang G B, Meng Y H, Zheng W, et al. Artificial frozen orbit control scheme based on J_2 perturbation. Sci China Tech Sci, 2010, 53(11): 3138–3144